Coupled Electromagnetic–Structural Simulation of Magnetic Pulse Welding

Angshuman Kapil and Abhay Sharma

Abstract The present study deals with the coupled magnetic–structural analysis of magnetic pulse welding (MPW) process applied on a tubular workpiece. The study investigates the various criteria required for a successful weld between the mating members through a finite element model. The transient electromagnetic field phenomenon is coupled sequentially with mechanical phenomenon. The coupling between the magnetic field and the electrical circuit is formulated in the electromagnetic part of the model, whereas in the structural part, the impact velocities, the effective plastic strain and the shear stress induced in the workpiece are found from the numerical simulations. A viscoplastic material model with rate-dependent material properties is considered in the structural part. The effect of varying process parameters: input voltage and air gap between the two mating members on weld quality are computed through numerical simulations. Based on the results of the numerical simulations, an optimal weldability window is suggested.

Keywords Magnetic pulse welding · Coupled magnetic–structural analysis · Finite element model · Weldability window

1 Introduction

Recent studies and advances in the welding fraternity have been made in order to develop a newer process which enables us to achieve better quality and productivity and is environment friendly. Magnetic pulse welding (MPW) is a step forward into the future of welding. In the recent years, the welding of dissimilar and lightweight

A. Kapil · A. Sharma (✉)
Department of Mechanical and Aerospace Engineering, Indian Institute of Technology
Hyderabad, ODF Campus, Yeddumailaram 502205, Telangana, India
e-mail: abhay@iith.ac.in

A. Kapil
e-mail: me13m0001@iith.ac.in

materials has been a topic of utmost interest for the researchers and industries. MPW is a potential candidate for joining of dissimilar materials (Raoelison et al. 2013). The process is quite effective and reliable in terms of cost and performance, respectively, having analogy to explosive welding (EXW) (Zhang et al. 2011). The entire process is contactless wherein a magnetic field helps generate the required magnetic pressure to drive the flyer tube/plate towards the base tube/plate by change of energy in electrical form to its mechanical form. The flyer workpiece driven with high velocities by the magnetic forces impacts against the base workpiece, and a weld is created as shown in Fig. 1. The feasibility of the welding depends upon the velocity of the flyer (Kore et al. 2010), the direction and magnitude of the shear stress in the weld zone and severe plastic deformation occurring on the surface of the mating members (Mousavi and Al-Hassani 2008). The weld length in MPW process is usually less than 1 cm, time needed for the formation of the bond is several microseconds, and the collision speed is of the order of several
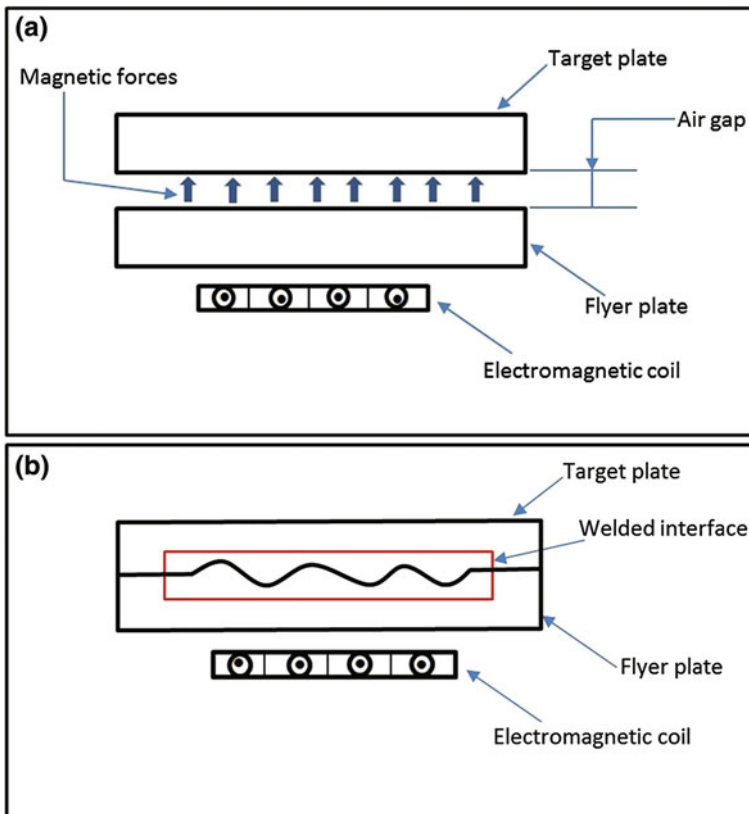
Fig. 1 Schematic illustration of MPW process: **a** initial MPW set-up for flat plates, **b** deformed geometry after the application of magnetic forces

hundreds of metres per second (Stern and Aizenshtein 2002). The temperature at the interface is always less than the melting point of the mating members.

There lies quite a few challenges for the modern day manufacturers; one of them being able to produce joints of high strength economically and without violating the strict environmental rules and regulations (Shribman 2007). One of the major problems faced by the manufacturers is the difficulty in joining dissimilar materials by the use of conventional joining processes. Dissimilarities in material properties such as temperature of melting, specific heat and coefficient of thermal expansion all prove to be a hindrance while attempting to join dissimilar materials. MPW is a substitute to conventional welding processes as the achievable weld joint strength is within the range of the strength of the weakest joining member (Weddeling et al. 2011).

With rapid advances in technology and demand for introduction of lightweight material concepts, the practice of using a single material does not seem feasible in many cases. Hence, a combination of different materials delivers the preferred technological characteristics required for the industries (Tomas 2010). Even though the process has been identified long back, there is a big scope for additional growth and application.

Successful application of MPW for tubular geometries dates back to 1969 (Zhang et al. 2011). Development of the process has made welding of tubular geometry highly successful and less cumbersome. In order to optimise the essential process parameters such as frequency, voltage, discharge energy and equivalent inductance, an electromagnetic field analysis is required. A finite element model (FEM) can allow the user to select optimum values of the parameters and help design the coil with suitable dimensions. The finite element modelling of MPW process requires coupling between electromagnetic and structural models. Very few works have been reported in the literature relating numerical modelling of tubes. Haiping et al. (2014) studied the influence of field shaper on quality of the weld as well as other process parameters such as air gap and input voltage. Zhidan et al. (2013) numerically computed the impact velocity during MPW of Al–Fe tubular geometry. Shim et al. (2010) investigated welding features taking into account the distributions of magnetic forces on the weldment using FEM to identify the ideal process parameters.

The present study deals with the numerical modelling of the MPW process applied to the tubes. The electromagnetic and structural models were coupled using FEM software 'COMSOL Multiphysics'. The feasibility of welding was investigated by studying three factors, viz. impact velocity, effective plastic strain and shear stress acting in the welded zone/impact zone based on published literature (Kore et al. 2010; Mousavi and Al-Hassani 2008). The impact velocity, effective plastic strain and shear stress along the weld zone were all determined from the numerical simulations. Based on the available literature, analytical calculations were done to determine the minimum impact velocity required for a successful weld to occur. The published literature also suggests minimum values of effective plastic strain and shear stress along the weld zone to determine the weldability of the joint. The feasibility of MPW of tubes was then ascertained by comparing the analytical

values of impact velocities, effective plastic strain and shear stress with the numerically computed values. The foregoing three criteria were calculated at various levels of process parameters, viz. input voltage and air gap between the mating members. Based on the varying process parameters and subsequent values of impact velocity, effective plastic strain and shear stress along the weld zone crossing a threshold value required for successful welding, a suitable weldability window for producing high weld length was reached upon.

2 Magnetic Pulse Welding: Process Components and Operating Principle

The MPW set-up consists mainly of four main units (Shribman 2007) with each unit having one or more than one component. Table 1 lists all the units and components of a general MPW set-up.

MPW is based on the principles given by Ampere which state that the force prevailing between two long parallel conductors of infinite length, separated from each other by distance 'd' and carrying currents I_1 and I_2 may be written as follows (Kore et al. 2007):

$$F = \frac{\mu_0}{2\pi d} I_1 I_2 \tag{1}$$

This force between the coil and the workpiece is repulsive in nature when the currents I_1 and I_2 move in directions opposite to each other and vice versa.

MPW is a very fast process with usual time taken for a cycle to complete being in microseconds. The process begins by charging the capacitors to the desired energy level. The workpieces are then positioned in the electromagnetic coil, and the trigger system operates the gap switch. Due to the closing of the switch, current

Table 1 Units and components of the MPW set-up (Shribman 2007)

Units	Components
Pulse generator	• Capacitor bank (inductance–capacitance circuit)
Control cabinet	• Power supply (DC power supply)
	• Spark gap (high voltage switch)
Workstation	• Work coils (actuators)
	• Workpieces
	- Flyer plate/tube
	- Target plate/tube
	• Field shaper (optional)
	• Electrical cables
Operational unit	• PLC
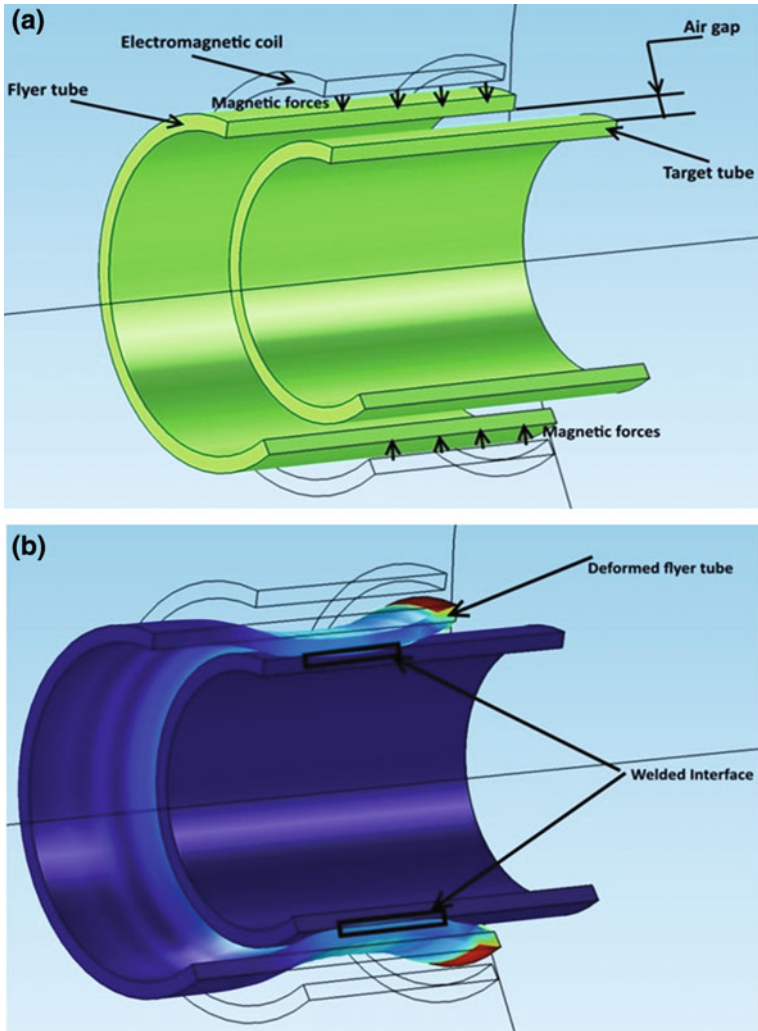
Fig. 2 MPW set-up for two tubes: **a** before the application of pulsed current, **b** after application of pulsed current

starts flowing rapidly through the coil, causing the magnetic flux to grow quickly from the coil winding and outward. This generates a magnetic field around the electromagnetic coil, and due to the secondary currents, i.e. eddy currents on the workpiece surface, a second magnetic field of opposite nature is generated as shown in Fig. 2.

The generated magnetic fields of opposing nature then interact with one other leading to the creation of a magnetic force field in between the coil and the workpiece. These magnetic forces, i.e. Lorentz forces, apply a magnetic pressure

and cause the flyer workpiece to collide with the base workpiece under very high velocities ranging in between 250 and 500 m/s (Aizawa et al. 2007; Epechurin 1974, 1978; Chudakov et al. 1980). The high velocity impact leads to plastic deformation of the mating members, and in certain circumstances, a solid-state weld is generated between the same.

3 Modelling for Analysis

3.1 Materials, Geometry and Process Parameters

In order to examine the process of MPW, structural steel ASTM A36 tubes were simulated as a 2D axisymmetric problem in the FEM. Table 2 shows the chemical composition of the material used in the model.

The investigated welding tests were typically composed of a hollow flyer tube and a hollow cylindrical base tube. The outer and inner diameters of the flyer tube were adjusted to calibrate the required air gap and are denoted as D2 and D1, respectively. The air gap between the tubes has been denoted by G. The arrangement of the flyer and the base tubes along with specific dimensions is shown in Fig. 3.

The outer and inner diameters of the base tube were kept fixed at 19 and 15 mm, respectively, for each of the test cases. The simulations were carried out at varying

Table 2 Chemical composition of structural steel ASTM A36 (ASTM Standard A36/A36M 2012)

Element	Composition (%)
Carbon, C	0.25–0.290
Copper, Cu	0.20
Iron, Fe	98.0
Manganese, Mn	1.03
Phosphorous, P	0.040
Silicon, Si	0.280
Sulphur, S	0.050

Fig. 3 Configuration of flyer and base tubes for different air gaps
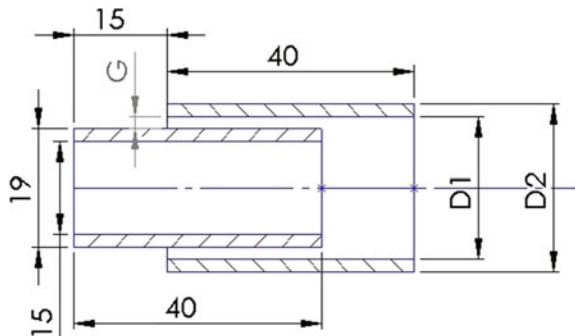
Table 3 Material properties and dimensions

Properties of flyer tube and target tube	Density (kg/m^3)		7850
	Ultimate tensile strength (MPa)		400–550
	Tensile yield strength (MPa)		250
	Modulus of elasticity (GPa)		200
	Bulk modulus (GPa)		140
	Shear modulus (GPa)		79.3
	Poisson's ratio		0.26
	Speed of sound (m/s)		4512
	Threshold value of impact velocity (m/s) (see Eq. 6)		297.7
	Threshold value of plastic strain Mousavi and Al-Hassani (2008)		0.35
	Threshold value of shear stress (GPa) Mousavi et al. (2005)		0.5
Properties of electromagnetic coil—copper	Relative permeability		1
	Resistivity (Ω m)		3.4×10^{-8}
	Inductance (H)		10^{-7}
Dimensions—flyer tube	Air gap (mm)	Outer diameter (mm)	Inner diameter (mm)
	0.5	24	20
	1	25	21
	1.5	26	22
	2	27	23
	2.5	28	24

process parameters. The process parameters which were varied for performing the simulations were air gap and input voltage. The input voltage was varied in steps of 0.5 kV from 6 to 9.5 kV and the air gap being varied from 0.5 to 2.5 mm in steps of 0.5 mm. The simulations were performed with a multi-turn copper coil. Properties of the copper coil are listed in Table 3. Table 3 also lists the material properties and dimensions of the flyer tube.

3.2 FEA Model of the MPW Process

The flowchart for a sequentially coupled Electromagnetic–Structural analysis is illustrated in Fig. 4. The physical environments, viz. electromagnetic and structural (electromagnetic coil, and flyer and base tubes, respectively) were established at first. The electromagnetic environment was then solved, which calculated the transient magnetic forces, i.e. Lorentz forces. These forces were fed as input load in the structural module to calculate the flyer tube's deformation at subsequent time steps. Based on the updated geometry of the tube, the time-dependent magnetic
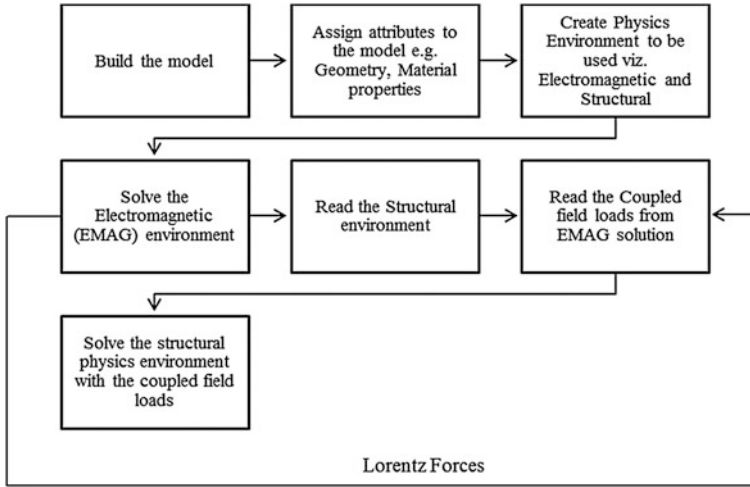
Fig. 4 Simulation flow chart for a sequentially coupled electromagnetic—structural analysis

forces were found out at subsequent time steps. The electromagnetic module consisted of the flyer and target tubes, the electromagnetic coil and a surrounding air region, whereas the structural module was related to the flyer, the target tubes and the coil. The structural module took into consideration the inertial effects because of time-dependent stress.

3.2.1 Governing Equations

In the tube region, Eq. (2) stated below is reached upon by substituting the constitutive equations into the equations given by Maxwell (Haiping and Chunfeng 2009):

$$\nabla \times \left(\frac{1}{\mu} \nabla \times \vec{A} \right) = -\Upsilon \frac{\partial \vec{A}}{\partial t} \tag{2}$$

where μ represents the permeability of the medium (H/m), Υ represents the conductivity of the medium (S/m), $-\Upsilon(\partial \vec{A}/\partial t)$ represents the current density (A/m^2) and $\vec{A}$ represents the magnetic vector potential.

The magnetic force $\vec{f}$ in unit volume of medium, i.e. the magnetic force density, is given by Maxwell's equation as follows (Haiping and Chunfeng 2009):

$$\vec{f} = \vec{J} \times \vec{B} = \frac{1}{\mu} \left(\nabla \times \vec{B} \right) \times \vec{B} \tag{3}$$

where $\vec{J}$ represents the coil current density (A/m^2) and $\vec{B}$ represents magnetic flux density (T).

The forces applied on the tube due to the generated magnetic fields can thus be calculated by substituting $\nabla \times \vec{A} = \vec{B}$ and Eq. (2) into Eq. (3) and the input body load in the structural module.

The load in the electromagnetic module is the current which passes through the electromagnetic coil, and this current is approximately expressed as follows (Haiping and Chunfeng 2009):

$$I = U\sqrt{\left\{\frac{C}{L}\exp(-\beta t)\sin(\omega t)\right\}} \tag{4}$$

where U represents the input voltage, C represents the capacitance, L represents the inductance, β represents the damping exponent and ω is the angular frequency.

The constitutive behaviour of the tube material is described by the default constitutive relation built in COMSOL, i.e. the Cowper–Symonds constitutive model (Haiping and Chunfeng 2009).

$$\sigma = \sigma_y \left[1 + \left(\frac{\dot{\varepsilon}}{P}\right)^m\right] \tag{5}$$

where σ_y represents the quasi-static flow stress, $\dot{\varepsilon}$ represents the plastic strain rate (s^{-1}), and P and m are specific material parameters.

3.3 Weld Validation Criteria

Three different criteria were investigated to ascertain the weldability of the joint, namely:

(a) Impact velocity
(b) Effective plastic strain
(c) Shear stress

(a) Impact velocity

The determination of impact velocity is a very essential step during MPW. Impact velocity determines the success of the weld. Available literature suggests analytical relations that give threshold values of impact velocity. The weld occurs as an when the threshold limit is crossed. Researchers have carried out extensive studies regarding the effect of impact velocity on the occurrence of weld. Separate relations have been suggested for similar and dissimilar material combinations.

Due to the absence of any specific criterion for MPW and the process being closely analogous to EXW, the criterion suggested by Kore et al. (2010) was used to obtain the minimum impact velocity required for a successful weld to occur in case of similar material combination. The relation is given as follows (Kore et al. 2010):

$$U = \left(\frac{\sigma_{TU}}{S}\right)^{1/2} \tag{6}$$

where U is the threshold velocity (m/s), σ_{TU} is the ultimate tensile stress (MPa) and S is the velocity of sound in the material considered (m/s).

Similarly for the case of dissimilar material combination, a different analytical relation was used to calculate the threshold value of impact velocity. The relation is given as follows (Botros and Groves 1980):

$$P = \frac{1}{2} Z_{eq} U \cos \Phi \tag{7}$$

where U is the required impact velocity for the occurrence of a successful weld, Z_{eq} is the equivalent acoustic impedance of the mating members, P is the critical impact pressure for jet formation and Φ is the critical angle for jet formation.

$$Z_{eq} = \frac{2}{1/z_1 + 1/z_2} \tag{8}$$

where

$$Z_1 = \rho_1 s_1 \text{ is the flyer tube acoustic impedance} \tag{9}$$

$$Z_2 = \rho_2 s_2 \text{ is the base tube acoustic impedance} \tag{10}$$

where ρ_1 and ρ_2 are the densities of the material considered and s_1 and s_2 are the speed of sound in the flyer and base tubes, respectively.

Apart from crossing the threshold impact velocity, there is a minimum value of impact pressure that also needs to be crossed to attain a successful weld. This is termed as the critical impact pressure and is determined by the relation (Botros and Groves 1980):

$$P = 5 \times \text{Hugoniot elastic limit (HEL)} \tag{11}$$

where HEL is given by the relation (Botros and Groves 1980):

$$\text{HEL} = \frac{1}{2}\left(\frac{K}{G} + \frac{4}{3}\right) Y_0 \tag{12}$$

where K is the bulk modulus, G is the shear modulus and Y_0 is the tensile yield stress.

In MPW, higher impact velocity leads to an increase in the impact pressure which causes severe plastic deformation at the weld interface of the mating members. The fundamental need of a successful weld is that the workpiece surfaces are free from the presence of any contaminants and oxide layers. Velocity of impact is the main parameter that causes variations in the bonding. Too high a velocity leads to formation of intermetallics at the weld interface which subsequently leads to brittle damage of the mating members. On the other hand at a very low velocity, the jet formed is unable to eliminate the contaminants and oxide layer from the workpiece surface leading to an unsuccessful weld.

The impact velocity is directly related to input voltage which in turn is related to discharge energy. The relation between discharge energy and input voltage is given in Eq. (13) (Raoelison et al. 2012). Increase in discharge energy leads to an increase in the energy of the workpiece (flyer) which subsequently increases the impact velocity.

$$E = CU^2/2 \tag{13}$$

where E represents the energy stored in the capacitors, C is the capacitance of the MPW system and U is the input voltage.

For every material arrangement, there is a certain level of energy essential for joining the metals and beyond a certain energy level weld does not occur (Kore et al. 2008).

The impact velocity required to conduct a successful weld between two structural steel ASTM A36 tubes was calculated to be 297.7 m/s from Eq. (6).

(b) Effective Plastic Strain

Available literature (Mousavi and Al-Hassani 2008) on MPW as well as EXW suggests that effective strain can be used as a possible criterion for bonding. Literature suggests a threshold value of effective plastic strain for bonding to take place. A value of 0.35 was suggested as the limiting value for bonding of steel to steel (Mousavi and Al-Hassani 2008).

(c) Shear Stress

Available literature (Mousavi et al. 2005; Mousavi 2008) suggests that shear stresses in the base and flyer tubes at the impact zone should be of opposite sign for successful welding. If the shear stresses in the weld interface were of the identical sign in the two mating members, welding was doubtful. A threshold value of 0.5 GPa was suggested to decide the weldability for stainless steel joints (Mousavi et al. 2005).

4 Results and Discussions

The numerical simulations to assess the weldability of the structural steel ASTM
A36 tubular assembly was carried out at various process parameters as mentioned
in the preceding section. The flyer tube was affected by both radial and axial forces
at a time, and thus, it suffered complicated stresses. The surface Von Mises stress
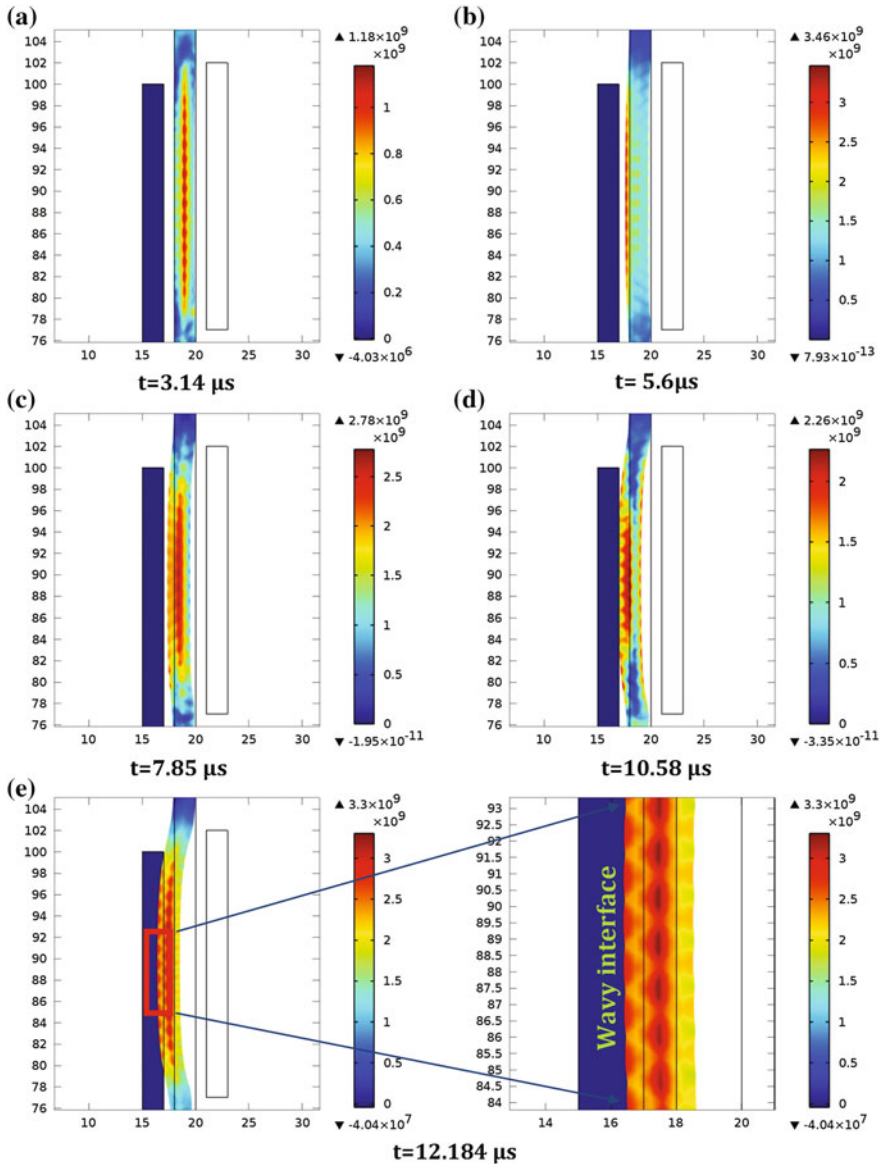developed in the flyer tube increased continuously with time (Fig. 5a–d) and

Fig. 5 Surface Von Mises stress at different times (input voltage—8.5 kV, air gap—1 mm)

reached the maximum value when the flyer tube collided with the target tube Fig. 5e. A wavy interface at the impact zone can be seen at the time of impact. The impact velocities, effective plastic strain and the shear stress at the time of impact were recorded for the 40 cases. The resulting weldability window and process mechanism are discussed in the succeeding section.

Figure 6a–c shows the comparison of three weldability criteria along the arc length at varying input voltages and a constant air gap of 1 mm. The arc length is the distance along the edge of the flyer plate at the impact zone. It can be observed that the impact velocity criterion could not be satisfied at 8 kV (Fig. 6a), whereas the effective plastic strain crossed the threshold at all the three input voltages (Fig. 6b). On the contrary, the shear stress criterion crossed the threshold at 8 kV but failed to do the same at 9 kV (Fig. 6c). The input voltage of 8.5 kV satisfied all the three criteria. Thus, the existence of process parameters which can satisfy all the three criteria in the MPW process was non-trivial.

The foregoing description was further extended to the remaining test cases and consolidated in Fig. 7. The pairs of the input voltage and the air gap are marked for the cases when an individual weldability criterion crossed the respective threshold value. It is seen that the plastic strain was the most versatile criteria that crossed the threshold limit followed by the impact velocity and the shear stress. The impact velocity crossed the threshold value at moderate and higher values of the investigated input voltage, whereas the same happened at moderate and lower values for the shear stress. The moderate input voltage except the minimal air gap of 0.5 mm was successful in crossing the threshold of the three criteria. Based on the above discussion, a weldability window was reached upon, as shown in Fig. 7. This window encompassed only those values of process parameters, where the impact velocity, effective plastic strain and shear stress together crossed their respective threshold values. The window identified the particular process parameters suitable for conducting a successful weld.

The process parameters that characterised the three weldability criteria were interrelated. The interrelation is explained through Fig. 8a–c that depicts the influence of process parameters on the impact velocity, the effective plastic strain and the shear stress, respectively.

From Fig. 8a, it is seen that the impact velocity increased with an increase in the input voltage. However, a minimum input voltage of 7.5 kV was essential to cross the threshold impact velocity. This is in agreement with the previously published observations (Zhidan et al. 2013) that one of the simplest ways to increase the quality of MPW is to increase the input voltage. At lower input voltages such as 6 and 6.5 kV, maximum impact velocity was obtained with the lowest air gap of 0.5 mm. A further increase in the input voltage at 0.5 mm air gap did not result in a significant amount of change in the impact velocity and eventually the flyer plate damaged at voltages ranging from 8 to 9.5 kV. The damage might be a result of low strain rate and high stress level that occurred at the time of discharge leading to crack initiation and propagation in the flyer (Raoelison et al. 2013). At a particular value of the air gap, the velocity and kinetic energy of the tubes reached a maximum value. Below this particular value, the tubes were unable to attain the
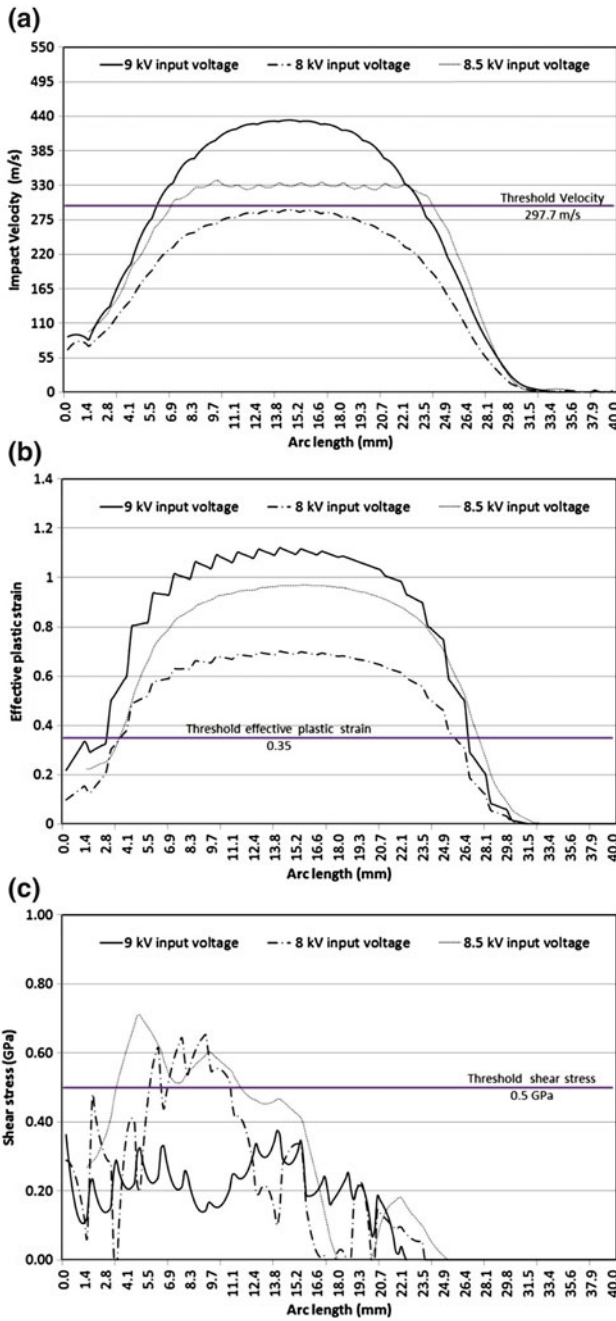
Fig. 6 Comparison of weldability criteria **a** impact velocity, **b** effective plastic strain, **c** shear stress (air gap = 1 mm)
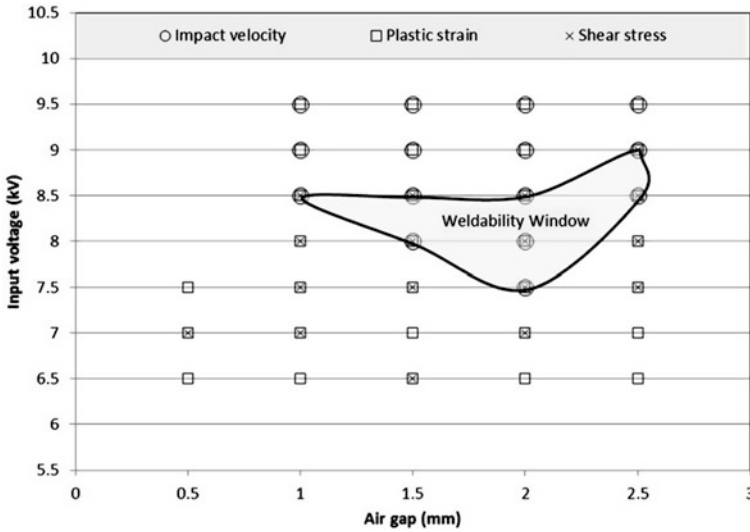
Fig. 7 Weldability window for MPW of structural steel ASTM A36

maximum possible velocity. At lower values of the air gap, e.g. 0.5 mm in the present case, the tubes collided well before the flyer attained the maximum velocity, whereas in case of larger air gaps, the velocity reached a value lower than the maximum at the time of the impact. The previously published experimental results (Kore et al. 2007) are in agreement with the observed numerical results in the present study.

As the input voltage was increased, the plastic strain induced in the members as well as the shear stress, increased up to an extent as shown in Fig. 8b, c, respectively. The increase of the input voltage led to an increase in the pressure acting upon the flyer tube. The pressure in the impact zone was mainly due to two phenomena: pressure induced due to the magnetic field and a pressure due to the impact intensity (Raoelison et al. 2012). High impact velocities produced high plastic deformation which subsequently resulted in higher levels of effective plastic strain at the impact zone. The numerically computed results suggest the existence of a plastic strain band, as well as a severely deformed impact zone with high values of plastic strain. The values of plastic strain crossed the threshold value for input voltages ranging from 6.5 to 9.5 kV suggesting that below 6.5 kV, the bonding would not take place (Fig. 8b). As the air gap was increased, the plastic strain values showed an increasing trend up to a certain value of input voltage and subsequently the value decreased. This confirms the presence of an optimum air gap (around 1.5 mm in the present case) between the members to achieve a good weld. At the lower air gap, it would not be possible to create a weld due to pressure deficiency, whereas at higher gaps, the impact would not take place.

The foregoing observation was also supported by the shear stress distribution shown in Fig. 8c. The shear stress values had opposite signs for the flyer and target
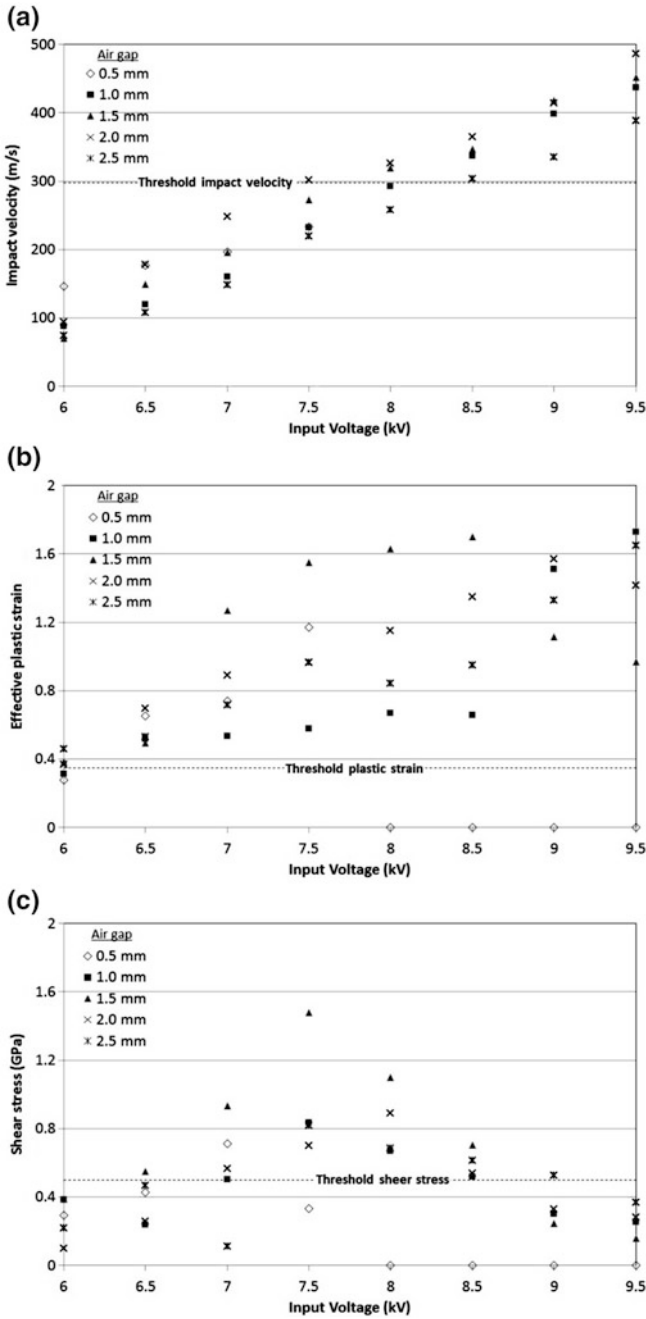
Fig. 8 Weldability criteria at different air gaps and input voltages **a** impact velocity, **b** effective plastic strain, **c** shear stress

tubes, respectively, for the cases where it crossed the threshold value of 0.5 GPa. At an input voltage of 6 kV, the shear stress value was below the threshold value for all the air gaps. From Fig. 8c, it can be observed that the shear stress crossed the threshold value for almost all air gaps at voltages ranging from 7 to 8.5 kV. Beyond this value of input voltage, the shear stress started to decrease and was unable to cross the threshold value. This would limit the allowable range of input voltage in a manner the impact velocity and the effective plastic strain would limit the allowable air gap as mentioned earlier.

The results of the present investigation emphasise on the need for an all-inclusive approach towards weldability criteria for MPW. Considering all, the three criteria would provide a more reliable range of process parameters to work with. Furthermore, use of FEM simulation would save the cost and the time spent in development of a product.

5 Conclusions

1. The three weldability criteria, namely impact velocity, effective plastic strain and the direction and magnitude of the shear stress studied in this investigation have a significant role in MPW of tubular joint.
2. Existence of process parameters which can simultaneously satisfy the three foregoing criteria is non-trivial. A comprehensive approach considering each of the foregoing weldability criteria for MPW should be adopted.
3. The process parameters in MPW are interrelated. A moderate input voltage at an optimum air gap could achieve a sound joint.
4. The demonstrated methodology of developing a weldability window through FEM simulation would save cost and time spent in production of product using MPW.

References

Aizawa T, Kashani M, Okagawa K (2007) Application of magnetic pulse welding for aluminum alloys and SPCC steel sheet joints. Weld J 86:119–124
Mousavi SAAA, Al-Hassani STS (2008) Finite element simulation of explosively-driven plate impact with application to explosive welding. Mater Des 29:1–19
Akbari Mousavi SAA, Burley SJ, Al-Hassani STS (2005) Simulation of explosive welding using the williamsburg equation of state to model low detonation velocity explosives. Int J Impact Eng 31:719–734
Akbari Mousavi SAA (2008) Numerical studies of explosive welding of three-layer cylinder composites-part 2. Mater Sci Forum 580–582:327–330
ASTM Standard A36/A36 M (2012) Specification for carbon structural Steel. ASTM International, West Conshohocken, PA doi:10.1520/A0036_A0036M-12

Botros KK, Groves TK (1980) Fundamental impact-welding parameters-an experimental investigation using a 76-mm powder cannon. J Appl Phys 51:3706–3714

Chudakov VA, Khrenov KK, Sergeeva YA, Gordan GN (1980) The effect of temperature to which the material is heated on the process of formation of intermetallic compound in magnetic pulse welding. Weld Prod 27(9):23–25

Epechurin VP (1978) Determination of the forces of the compressive effect in nonmagnetic multilayer conductors. Power Eng 16(3):115–120

Epechurin VP (1974) Properties of bimetal joints by magnetic pulse welding. Weld Prod 21(5):4–12

Haiping YU, Chunfeng LI (2009) Effects of current frequency on electromagnetic tube compression. J Mater Process Tech 209:1053–1059

Haiping YU, Zhisong F, Chunfeng LI (2014) Magnetic pulse cladding of aluminum alloy on mild steel tube. J Mater Process Tech 214:141–150

Kore SD, Date PP, Kulkarni SV (2008) Electromagnetic impact welding of aluminum to stainless steel sheets. J Mater Process Tech 208:486–493

Kore SD, Date PP, Kulkarni SV (2007) Effect of process parameters on electromagnetic impact welding of aluminum sheets. Int J Impact Eng 34:1327–1341

Kore SD, Dhanesh P, Kulkarni SV, Date PP (2010) Numerical modeling of electromagnetic welding. Int J Appl Electrom 32:1–19

Raoelison RN, Buiron N, Rachik M, Haye D, Franz G (2012) Efficient welding conditions in magnetic pulse welding process. J Manuf 14:372–377

Raoelison RN, Buiron N, Rachik M, Haye D, Franz G, Habak M (2013) Study of the elaboration of a practical weldability window in magnetic pulse welding. J Mater Process Tech 213:1348–1354

Shim JY, Kang BY, Kim IS, Kang MJ, Park DH, Kim IJ (2010) A study on distributions of electromagnetic force of the dissimilar metal joining in MPW using a FEM. Adv Mat Res 83–86:214–221

Shribman V (2007) Magnetic pulse welding of automotive HVAC parts. Pulsar—Magnetic pulse solutions, pp 1–31

Stern A, Aizenshtein M (2002) Bonding zone formation in magnetic pulse welds. Sci Technol Weld Joi 7(5):339–342

Tomas BMC (2010) Magnetic pulse welding MPW. Ph. D. thesis, Department of Mechanical Engineering Universidade Nova de Lisboa, Portugal

Weddeling C, Woodward ST, Marre M, Nellesen J, Psyk V, Tekkaya AE, Tillmann W (2011) Influence of groove characteristics on strength of form-fit joints. J Mater Process Tech 211:925–935

Zhang Y, Babu SS, Prothe C, Blakely M, Kwasegroch J, LaHa M, Daehn GS (2011) Application of high velocity impact welding at varied different length scales. J Mater Process Tech 211:944–952

Zhidan XU, Junjia C, Haiping YU, Chunfeng LI (2013) Research on the impact velocity of magnetic impulse welding of pipe fitting. Mater Des 49:736–745